ADVANCED FUNCTIONAL MATERIALS

FULL PAPER

DOI: 10.1002/adfm.200600663

Tuning the Energy Level and Photophysical and Electroluminescent Properties of Heavy Metal Complexes by Controlling the Ligation of the Metal with the Carbon of the Carbazole Unit**

By *Chuluo Yang*,* *Xiaowei Zhang*, *Han You*, *Lingyun Zhu*, *Lianqing Chen*, *Linna Zhu*, *Youtian Tao*, *Dongge Ma*,* *Zhigang Shuai*,* and *Jingui Qin**

Four novel Ir^{III} and Pt^{II} complexes with cyclometalated ligands bearing a carbazole framework are prepared and characterized by elemental analysis, NMR spectroscopy, and mass spectrometry. Single-crystal X-ray diffraction studies of complexes **1**, **3**, and **4** reveal that the 3- or 2-position C atom of the carbazole unit coordinates to the metal center. The difference in the ligation position results in significant shifts in the emission spectra with the changes in wavelength being 84 nm for the Ir complexes and 63 nm for the Pt complexes. The electrochemical behavior and photophysical properties of the complexes are investigated, and correlate well with the results of density functional theory (DFT) calculations. Electroluminescent devices with a configuration of ITO/NPB/CBP:dopant/BCP/AlQ_3/LiF/Al can attain very high efficiencies.

1. Introduction

Organic light-emitting diodes (OLEDs) continue to attract intensive interest because of their numerous applications in full-color flat-panel displays and other lighting sources.[1] Of all the materials used as emitters in OLEDs, phosphorescent heavy metal complexes, such as Ir^{III},[2] Pt^{II},[3] Os^{II},[4] Ru^{II},[5] and Re^{I}[6] complexes, are the most promising candidates as their strong spin–orbital coupling induces an efficient intersystem crossing from the singlet to the triplet excited state, which enables them to utilize both excited states, and, therefore, the internal quantum efficiency can theoretically approach 100 %.[7]

A multilayer architecture consisting of a hole-transporting (HT), an electron-transporting (ET), and an emissive layer is generally adopted to achieve a balanced injection and transport of holes and electrons, which is essential for a high-efficiency OLED device.[8] Thus, it would be reasonable to have phosphorescent complexes embrace structural features for optimizing charge transport across the bulk. This strategy has been proven to be effective in enhancing the device efficiency of OLEDs based on lanthanide complexes.[9] Most recently, research endeavors have involved the use of aromatic amines (as HT layers) and/or oxadiazoles (as ET layers) in the design of iridium or platinum complexes.[10]

The emission frequency of the heavy metal complexes can usually be tuned by changing the electronic nature and/or position of the substituents on the ligands. For example, the emission wavelengths of the iridium complexes can cover the whole visible region by modification or variation of cyclometalated 2-arylpyridine ligands.[11] Since the emission of these phosphorescent complexes generally originates from metal-to-ligand charge-transfer (MLCT), which is controlled by both the ligands and the metal ions, an alternative route for emission tuning is to use different metal centers for a given ligand; surprisingly, the related reports are very limited.[12]

Carbazole-based compounds have played a very important role in organic/polymeric optoelectronic materials. In OLEDs carbazole derivatives can usually be used as host materials for both small-molecule OLEDs (such as 4,4′-*N*,*N*′-dicarbazole-biphenyl, CBP) and polymer OLEDs (such as poly(vinylcarbazole), PVK) because of their high triplet energy and good hole-transporting ability.[2a,13] The carbon atoms at the 2/7 and 3/6 positions of carbazole have a different electronic density,

[*] Prof. C. L. Yang, Prof. J. G. Qin, X. W. Zhang, L. Q. Chen, L. N. Zhu, Y. T. Tao
Department of Chemistry, Hubei Key Lab on Organic and Polymeric Optoelectronic Materials, Wuhan University
Wuhan 430072 (P.R. China)
E-mail: clyang@whu.edu.cn; jgqin@whu.edu.cn
Prof. D. G. Ma, H. You
State Key Laboratory of Polymer Physics and Chemistry
Changchun Institute of Applied Chemistry
Chinese Academy of Sciences
Changchun 130022 (P.R. China)
E-mail: mdg1014@ciac.jl.cn
Prof. Z. G. Shuai, L. Y. Zhu
CAS Key Laboratory of Organic Solids, Institute of Chemistry
Chinese Academy of Sciences
Beijing 100080 (P.R. China)
E-mail: zgshuai@iccas.ac.cn

[**] This work was supported by the National Natural Science Foundation of China (Project Nos. 20371036 and 20474047), the Program for New Century Excellent Talents in University, the Ministry of Education of China, the Ministry of Science and Technology of China through the 973 program (Grant No. 2002CB613406).

whereby the carbon atoms at the 3/6 position are activated by the nitrogen atom and thus more electron-rich than those at the 2/7 position.[14] The energy level of carbazole-based compounds can thus be tuned by substitution at the 3/6 or 2/7 positions.[15] Carbazole derivatives that are substituted or connected at the 3/6 position have been widely investigated. However, the 2/7-substituted carbazole-based compounds have not received attention until recently.[16] Moreover, there has not been any report to date involving metal complexation by ligation of the metal with the carbon of a carbazole unit.

In this work, we report the design and synthesis of two novel carbazole-based ligands and their corresponding cyclometalated Ir^{III} and Pt^{II} complexes. We expect that the ligation of different metals with the C-2 and C-3 position of carbazole would result in different bandgaps of the MLCT in these complexes, in consequence the photophysical properties of the complexes could be tuned. In addition, the carbazole fragment was included as a part of the ligand framework in order to improve the hole-transporting ability, and consequently to facilitate the charge injection and transporting in the electroluminescence process for high-performance OLEDs.

2. Results and Discussion

2.1. Synthesis and Characterization

As shown in Scheme 1, two carbazole-based ligands, 2-pyridinyl-*N*-ethylcarbazole (2-PEC) and 3-pyridinyl-*N*-ethylcarbazole (3-PEC) were prepared from the corresponding bromo-substituted carbazole and 2-bromopyridine by a Negishi cross-coupling reaction. The cyclometalated iridium and platinum complexes were synthesized in two steps. The ligands were first reacted separately with $IrCl_3$ and K_2PtCl_4 to give the corresponding cyclometalated μ-chloro-bridged dimers.[17] Subsequent treatment of the dimers with acetylacetone in the presence of Na_2CO_3 afforded the desired phosphorescent complexes, Ir(2-PEC)$_2$(acac) (**1**), Ir(3-PEC)$_2$(acac) (**2**), Pt(2-PEC)(acac) (**3**), and Pt(3-PEC)(acac) (**4**).

All the complexes were fully characterized by NMR, elemental analysis, and mass spectroscopy. The ^{1}H NMR data of two iridium complexes indicate symmetry in the complexes, suggesting that the iridium centers are coordinated by the two cyclometalated ligands with *cis*-C,C and *trans*-N,N conformation. The molecular structure of **1**, **3**, and **4** were further identi-

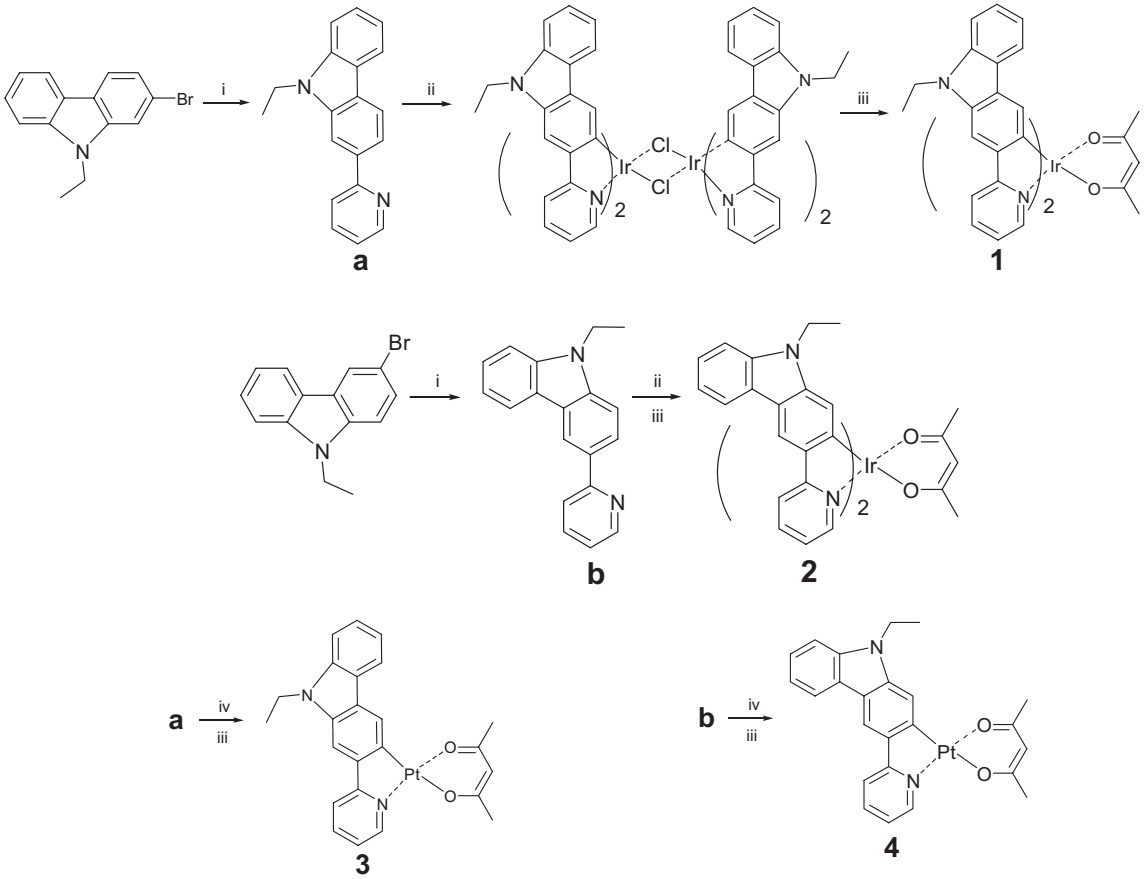

Scheme 1. Synthesis of the complexes **1**–**4**. **a**: 2-PEC; **b**: 3-PEC; **1**: Ir(2-PEC)$_2$(acac); **2**: Ir(3-PEC)$_2$(acac); **3**: Pt(2-PEC)(acac); **4**: Pt(3-PEC)(acac). Reaction conditions: i) 2-bromopyridine, *n*-BuLi –78 °C, $ZnCl_2$, $Pd(PPh_3)_4$, THF; ii) $IrCl_3 \cdot n\,H_2O$, 2-ethoxyethanol/H_2O; iii) acetylacetone, Na_2CO_3, 2-ethoxyethanol; iv) K_2PtCl_4, 2-ethoxyethanol/H_2O.

ADVANCED FUNCTIONAL MATERIALS

fied by using single-crystal X-ray crystallography. All the complexes are air-stable and sublimable. Thermal gravimetric analysis (TGA) in nitrogen shows that the decomposition temperatures of these complexes are all above 300 °C, which is beneficial to the long-term stability of OLED devices fabricated from these materials.

2.2. Crystal Structures of 1, 3, and 4

Single crystals of complexes **1**, **3**, and **4**, obtained by slow diffusion of diethylether to a dilute dichloromethane solution of the complex, were analyzed by X-ray crystallography. Molecular structures of the three complexes (Oak Ridge thermal ellipsoid plot (ORTEP) drawing) are shown in Figures 1–3. Selected important bond distances and bond angles are given in Table 1. Ir(2-PEC)$_2$(acac) (**1**) exhibits an octahedral coordination geometry around the Ir center with *cis*-C,C and *trans*-N,N dispositions. The Ir–C bonds (Ir–C_{av} = 2.001(6) Å) are shorter than the Ir–N bonds (Ir–N_{av} = 2.039(5) Å). Two platinum complexes (**3** and **4**) have a somewhat distorted square planar geometry: the Pt–C bonds (Pt–C = 1.974(4) Å for **3** and 1.974(6) Å for **4**) are shorter than the Pt–N bonds (Pt–N = 1.988(4) Å for **3** and 1.995(5) Å for **4**). All other features for all the complexes appear to be analogous to previous reports on similar types of complexes.[3d,11,18] As we expected for the ligand of the 2-PEC complex, the 3-position C atom of the carbazole part coordinates to the metal center (Fig. 1 and 2), while in the case of the ligand of the 3-PEC complex, the 2-position C atom chelates with the metal center (Fig. 3). The coordination models provide us with an access point to studying how chelating C atoms with different electronic densities influence the energy gap of the whole metal complexes.

Table 1. Selected structure parameters ([Å], [°]) for complexes **1**, **3**, and **4**.

Complex	1	3	4
M-C [a]	1.999(6)	1.974(4)	1.974(6)
	2.002(5)		
M-N	2.028(5)	1.988(4)	1.995(5)
	2.050(5)		
M-O	2.170(4)	2.004(3)	1.993(4)
	2.179(4)	2.083(3)	2.086(4)
C-M-C	91.1(2)		
N-M-N	177.11(18)		
O-M-O	87.08(15)	92.33(13)	91.79(18)
C-M-O	90.53(18)	93.20(16)	92.3(2)
	91.66(18)	174.43(16)	175.7(2)
	175.48(19)		
	174.8(2)		
N-M-O	88.59(17)	174.55(15)	173.84(19)
	85.27(16)	93.11(15)	94.1(2)
	94.29(17)		
	94.77(17)		
C-M-N	96.5(2)	81.36(17)	81.8(3)
	81.3(2)		

[a] M represents Ir or Pt.

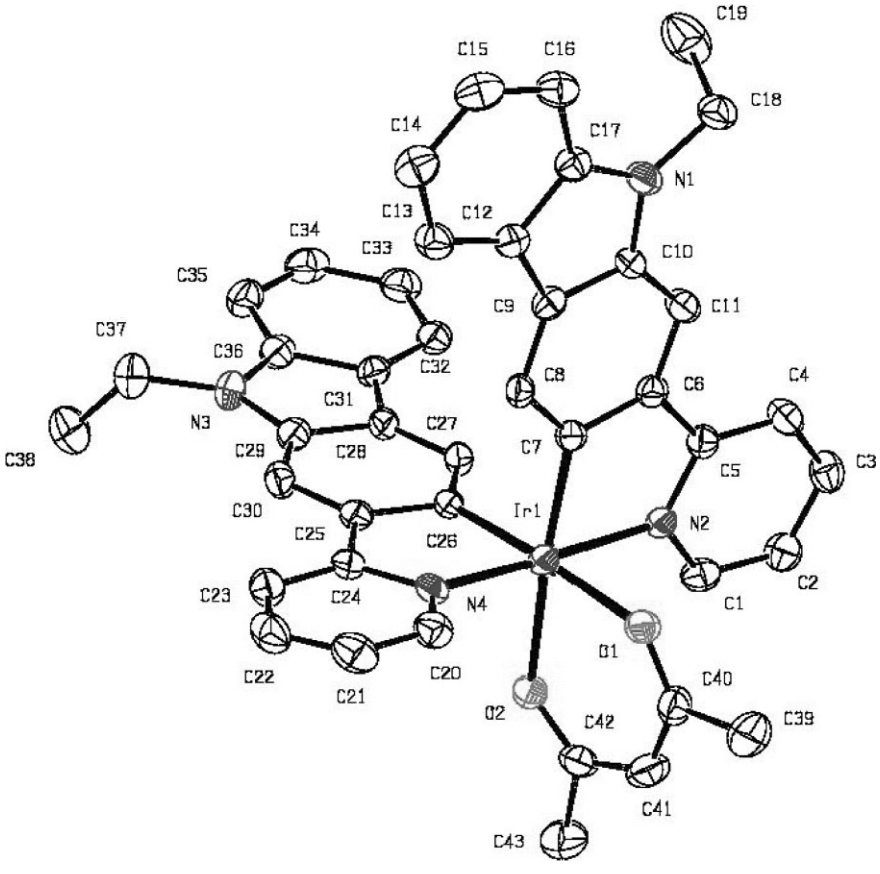

Figure 1. ORTEP diagram of the complex Ir(2-PEC)$_2$(acac) (**1**).

Interesting intermolecular interactions have been observed in the two platinum complexes. From the crystal-packing diagrams (Fig. 4 and 5), the molecules pack as head-to-tail dimers in both complexes. Complex **4** has a smaller plane-to-plane separation (3.287 Å) and Pt–Pt distance (3.6110 Å) than complex **3** (3.557 Å and 4.0195 Å, respectively), indicating that **4** has stronger intermolecular interactions than **3** in the solid state. The effect of the intermolecular contacts on the luminescent properties of platinum complexes will be discussed in the section of photoluminescence (PL) and electroluminescence (EL).

2.3. Photophysical Properties

Figure 6 shows the absorption and photoluminescence spectra of the four complexes in dichloromethane solution at room temperature. The spectral data are given in Table 2. The intense absorption peaks in the ultraviolet region of the spectra, between 250 and 350 nm, are attribut-

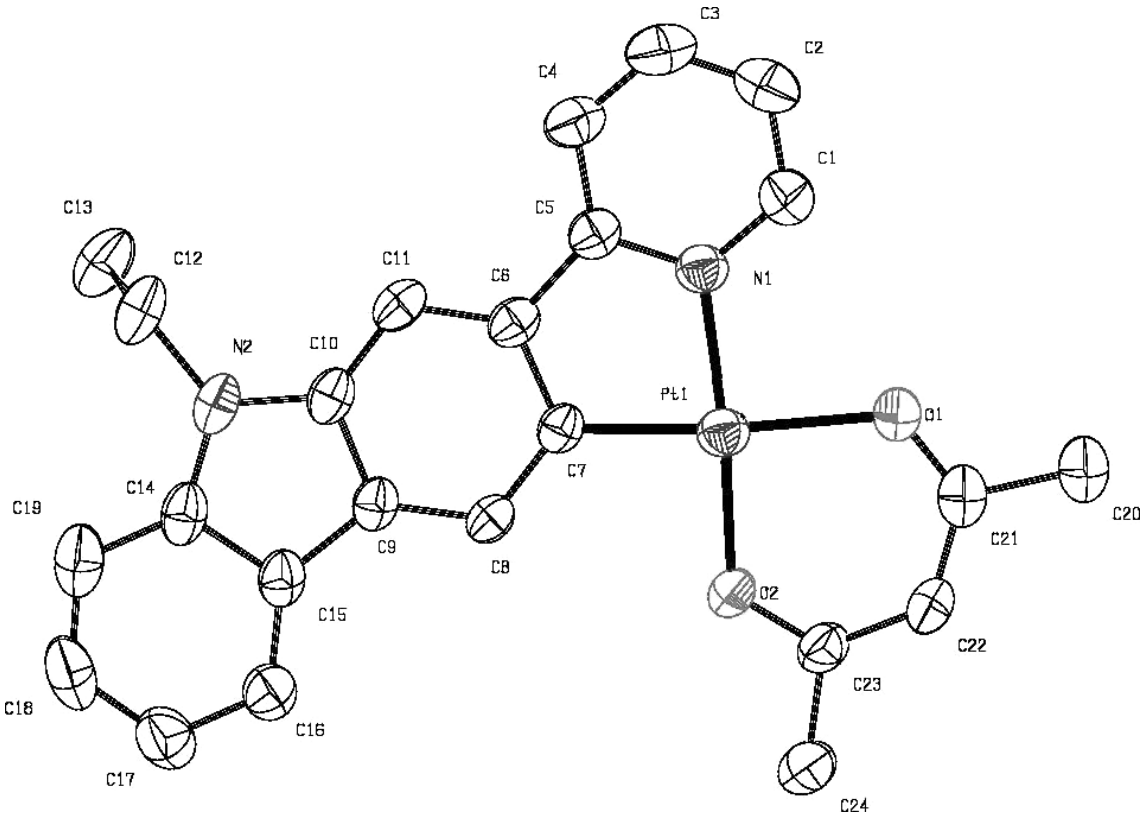

Figure 2. ORTEP diagram of the complex Pt(2-PEC)(acac) (**3**).

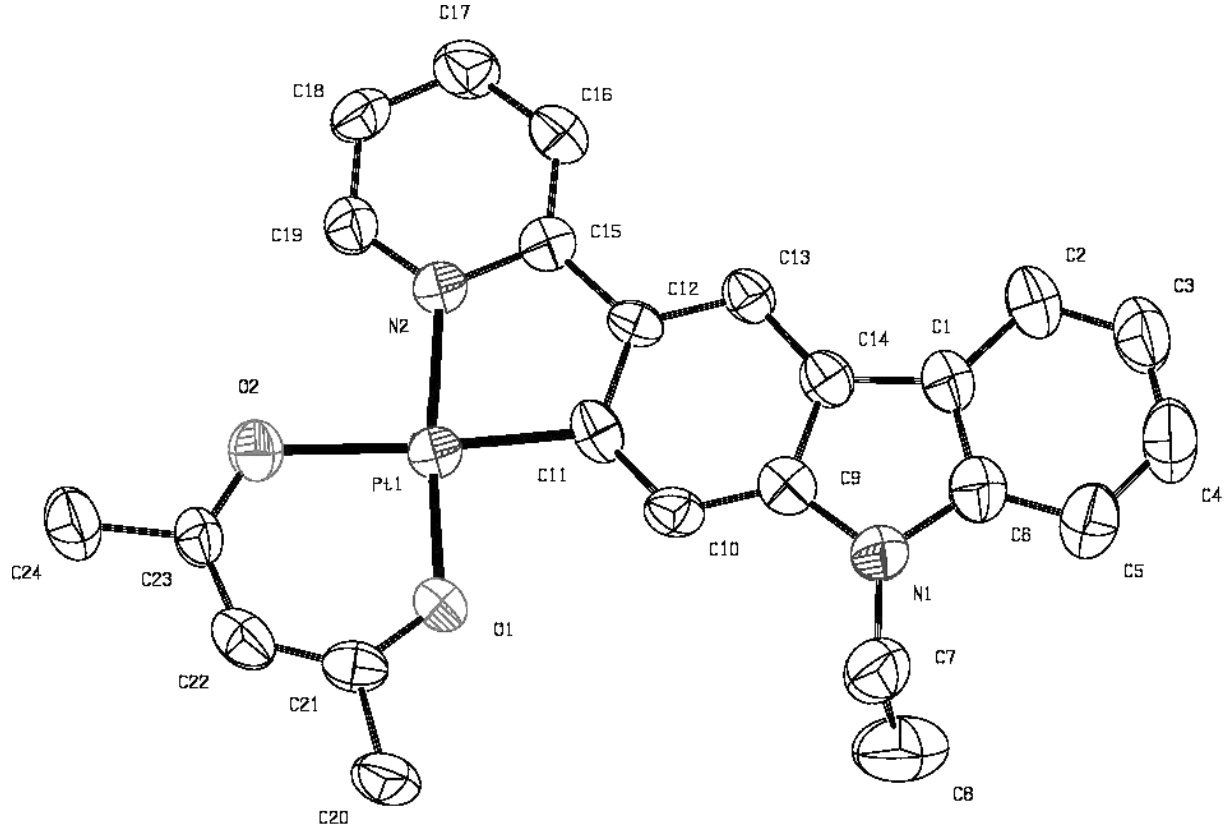

Figure 3. ORTEP diagram of the complex Pt(3-PEC)(acac) (**4**).

ADVANCED FUNCTIONAL MATERIALS

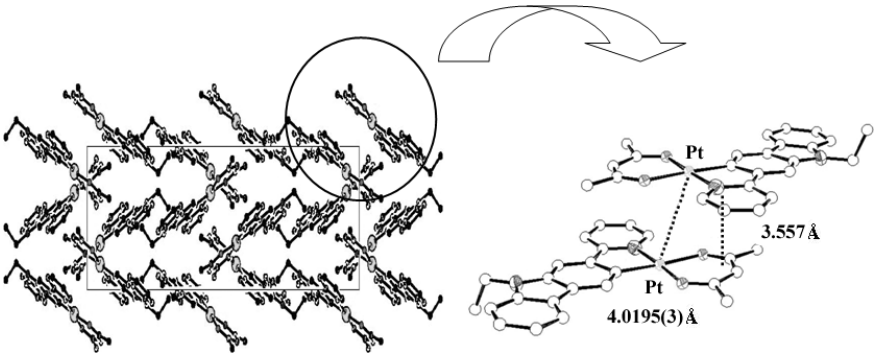

Figure 4. Crystal packing diagrams of **3**, illustrating intermolecular interactions.

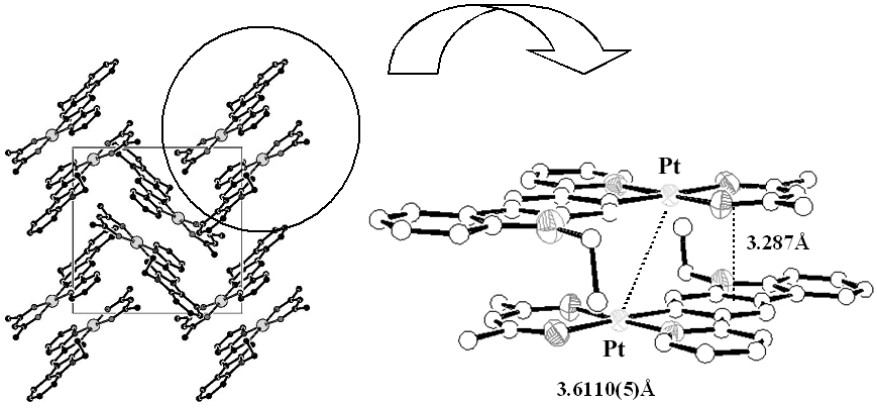

Figure 5. Crystal packing diagrams of **4**, illustrating intermolecular interactions.

Table 2. Photophysical and electrochemical data for complexes.

Complex	λ_{abs} [nm] (log ε) [a]	λ_{em} [nm] [a]	Φ [b]	$E_{1/2}^{ox}$ [V] [c]	HOMO [eV] [d]	LUMO [eV] [e]
1	289 (5.0), 344 (5.0), 478 (3.8), 518 (3.9)	594	0.02	–0.04	–4.69	–2.30
2	323 (5.2), 420 (4.0), 453 (3.9)	511	0.22	0.15	–4.88	–2.02
3	274 (4.6), 335 (4.5), 383 (4.2), 452 (3.6)	560	0.19	0.13	–4.91	–2.49
4	299 (4.9), 326 (4.8), 373 (4.3), 400 (4.1)	493 (526)	0.16	0.21	–5.03	–2.34

[a] Measured in dichloromethane solution. [b] The relative quantum yields were calculated relative to $(ppy)_2Ir(acac)$. [c] Potential values are reported versus Fc/Fc^+. [d] Determined from the onset oxidation potential. [e] Determined from the onset reduction potential.

ed to transitions of ligand-centered states with mostly spin-allowed $^1\pi$–π^* character because their energies and extinction coefficients are comparable to those of the corresponding free ligands. Low-energy transitions that extend to the visible region are conventionally assigned to a spin-allowed singlet metal-to-ligand charge transfer (^{1}MLCT) band and spin-forbidden ^{3}MLCT transitions. The high intensity of MLCT, with extinction coefficients between 4000 and 12 000 $M^{-1}cm^{-1}$, attributes to an efficient mixing of these charge-transfer transitions with a high spin-allowed $^1\pi$–π^* transition of cyclometalated ligands through the spin–orbit coupling on the heavy metal center.[19] Complex **1** exhibits significantly lower energy absorptions (extending to ca. 550 nm) than complex **2** (extending to ca. 500 nm). Likewise, complex **3** exhibits lower energy transitions (extending to ca. 500 nm) than complex **4** (extending to ca. 450 nm).

The PL spectrum of **1** in dichloromethane shows an emission peak at 595 nm, which falls in the orange–red region, while **2** emits green light with an emission maximum at 511 nm. A wavelength tuning of 84 nm is achieved. Complex **3** in dichloromethane shows an emission peak at 560 nm, which falls in the yellow–orange region, while complex **4** shows blue–green light with an emission maximum at 493 nm. There is also a difference of 67 nm between their maximal emissions. This remarkable difference of emission wavelengths is consistent with the difference of ^{3}MLCT absorptions of the complexes, implying that the emissions come from the triplet excited-state phosphorescence. For the ligands of 2-PEC and 3-PEC, the platinum complexes show hypsochromic shifts of 34 and 18 nm, respectively, compared to their iridium counterparts. In comparison with the PL spectra in solution, the PL spectra of two iridium complexes in a solid neat film show red-shifts of 9 nm (**1**) and 27 nm (**2**), respectively, while for the two platinum complexes, the excimer emissions in the film become dominant due to the easy aggregation of square-planar platinum complexes as displayed in their crystal structures.

2.4. Density Functional Theory (DFT) Calculations

To understand the remarkable color tuning of the four complexes, density functional theory (DFT) and time-dependent DFT (TDDFT) calculations were carried out using B3LYP hybrid functional theory (for details, see the Experimental section). The contour plots depicted in Figure 7 show that the highest occupied molecular orbitals (HOMOs) are basically comprised of a mixture of carbazole parts of the ligand and metal orbitals, while the lowest unoccupied molecular orbitals (LUMOs) are mainly localized on the pyridine moiety of the ligand frame. The calculated excited energies from

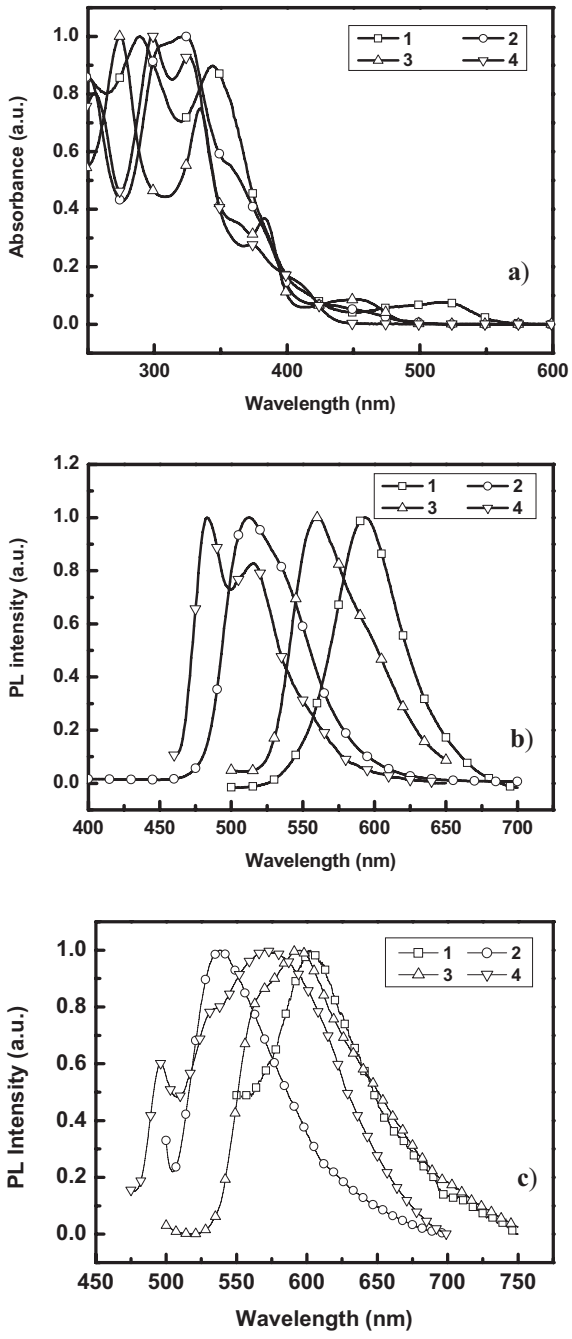

Figure 6. a) Absorption and b,c) PL spectra of the complexes in CH_2Cl_2 solution (b) or neat film (c).

the ground state to the first triplet excited states are 2.23 eV for **1**, 2.55 eV for **2**, 2.23 eV for **3**, and 2.57 eV for **4**, which correspond to emission wavelengths of 556 nm for **1**, 486 nm for **2**, 556 nm for **3**, and 482 nm for **4**. The values for the two platinum complexes correlate well with the phosphorescence peak wavelengths of the experimental data (see before). The emission peaks of the two iridium complexes show a bathochromic shift in comparison with the theoretical values, presumably because of the solvent stabilization.[20]

2.5. Electrochemical Analysis

The electrochemical properties of the complexes were examined using cyclic voltammetry, and the redox data are given in Table 2. All of the electrochemical potentials were measured relative to an internal ferrocene reference (Fc/Fc^+). The four complexes all undergo a single reversible oxidation wave ranging from –0.04 to 0.21 V during an anodic scan in CH_2Cl_2. These values are all in the range of those reported for $Ir(ppy)_2(acac)$ (ppy = 2-phenylpyridine),[21] Pt(ppy)(acac),[3d] and analogues.[19] During a cathodic sweep in tetrahydrofuran (THF), only $Ir(2\text{-PEC})_2(acac)$ exhibits a quasi-reversible reduction wave, the other three show irreversible reduction processes. Based on the onset potentials of the oxidation and reduction, the HOMO and LUMO energy levels of these complexes could be estimated with regard to the energy level of ferrocene (4.8 eV below vacuum). As shown in Table 2, the 3-position carbazole-ligated complexes, **1** and **3**, have higher HOMO and lower LUMO levels than their corresponding 2-position ligated complexes, **2** and **4**, respectively. This electrochemical behavior is in agreement with the description of a pyridine-localized LUMO and HOMO with substantial metal character, as seen in the above DFT calculations. The more electron-donating 3-position carbon of carbazole will destabilize the metal *d* orbital when ligating to the metal, leading to a higher HOMO than that of the less electron-donating 2-position. In contrast, the connection of pyridine with the carbon at the less electron-rich 2-position of the carbazole unit stabilizes the LUMO (pyridine-moiety localized) more than the connection at the 3-position. The two factors work together to narrow the energy gap of the complexes with the ligand 2-PEC. This corresponds to a bathochromic shift in the emission of the 2-PEC-based complexes (**1** and **3**) relative to the corresponding 3-PEC-based complexes (**2** and **4**) (see before).

2.6. Electrophosphorescent Properties

The electrophosphorescent properties of the four complexes were studied by using them as dopants in the emission layer of OLEDs. The device configuration is similar to that developed by Forrest and Thompson.[2a] ITO/NPB(400 Å)/dopant:CBP-(300 Å)/BCP(200 Å)/AlQ_3(300 Å)/LiF(10 Å)/Al(1000 Å), in which 4,4′-biscarbazolybiphenyl (CBP) serves as the host for metal complexes, 2,9-dimethyl-4,7-diphenyl-1,10-phenanthroline (BCP) as the hole and exciton blocker, and 4,4′-bis[*N*-(1-naphthyl)-*N*-phenylamino]biphenyl (NPB) and tris(8-hydroxyquinoline)aluminum (AlQ_3) as the hole-transporting and electron-transporting materials, respectively.

Table 3 summarizes the EL performance of all devices. As for the iridium complexes, all the devices based on **1** exhibited bright-red emissions at 608 nm with Commission Internationale de l'Eclairage (CIE) coordinates (*x*, *y*) of (0.63, 0.37), and those based on **2** displayed bright green emissions at 516 nm with CIE coordinates of (0.29, 0.63). The devices based on the two iridium complexes showed a different dependence on

ADVANCED FUNCTIONAL MATERIALS

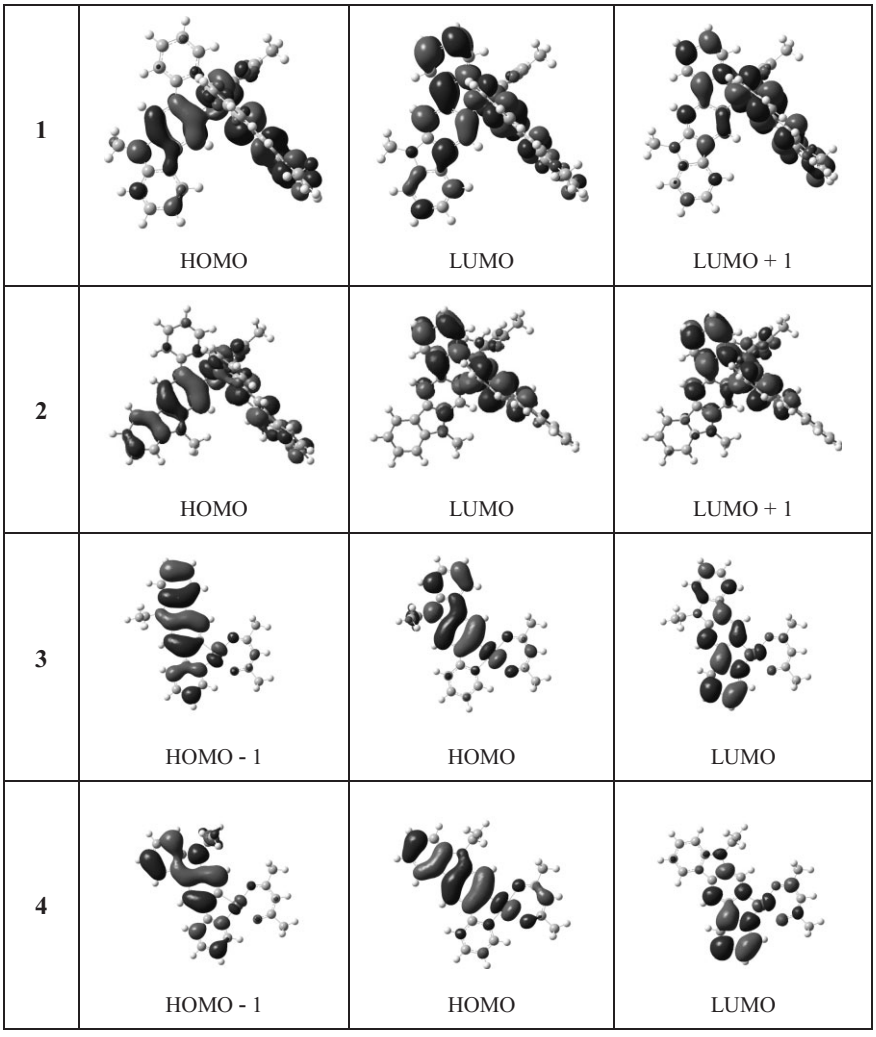

Figure 7. Contour plots of dominant excitation orbitals of the complexes.

the doping concentration (Fig. 8). For complex **2**, the device with 7 wt % doping concentration exhibited a much better performance than that with 3 wt % doping concentration. The 7 wt %-doped device has a turn-on voltage of only 3.1 V, and a maximum luminance (L_{max}) of 25 811 Cd m^{-2} at a current density (J) of 222 mA cm^{-2}. The maximum luminance efficiency ($\eta_{c,max}$) and power efficiency ($\eta_{p,max}$) are 31.60 Cd A^{-1} at $J = 0.95$ mA cm^{-2} and 19.03 lm W^{-1} at $J = 0.007$ mA cm^{-2}, respectively. On the contrary, for complex **1**, the device with 3 wt % doping concentration shows a significantly better performance than that with 7 wt % doping concentration. The 3 wt %-doped device displayed a high performance with $\eta_{c,max}$, $\eta_{p,max}$, and L_{max} of 12.18 Cd A^{-1} at $J = 0.43$ mA cm^{-2}, 4.63 lm W^{-1} at $J = 0.25$ mA cm^{-2}, and 8926 Cd m^{-2} at $J = 264$ mA cm^{-2}, respectively. This phenomenon suggests that the device with the red-emitting complex **1** as the phosphorescent dye is more prone to concentration saturation than that with the green-emitting complex **2**.

Whereas the EL spectra of the iridium complexes are independent of the doping concentration, the EL spectra of the platinum complexes changed with the doping concentration due to the excimer emission (Fig. 9 and 10). To the devices based on complex **3**, the EL spectrum resembles the PL spectrum at 2 wt % doping level. When the doping concentrations increases, two shoulders at around 600 and 666 nm, which are usually assigned to the excimer emission,[18] appear and gradually increase in intensity. The highest radiance (10 265 Cd m^{-2} at 190 mA cm^{-2}, λ_{max} 560 nm, CIE coordinates $x = 0.48$, $y = 0.48$), the maximum luminance efficiency (35.82 Cd A^{-1} at 0.01 mA cm^{-2}), and power efficiency (25.00 lm W^{-1} at 0.01 mA cm^{-2}) are achieved by using emitter **3** at 4 wt % doping level (Fig. 11). To the best of our knowledge, this is the best performance among Pt^{II} complex-based OLED devices.[3d,22] The luminance efficiencies are comparable to those obtained for iridium electrophosphorescent materials.[11] For the devices using complex **4** as dopant at a 2 wt % ratio, emission from CBP at λ_{max} ca. 450 nm was obtained, which indicates an insufficient energy transfer from the host CBP to the dopant. At 5 wt % ratio, the emission appearance is close to the PL spectrum. A radiance of 1624 Cd m^{-2} and efficiency of 3.51 Cd A^{-1} are obtained for a green-light-emitting device based on complex **4**. At 8 wt % and 10 wt % ratio, the emission intensities from the excimer exceed those from the monomer, which results in very broad spectra (Fig. 10). This characteristic can be used to fabricate white-light OLEDs by using excimer emission from a phosphor dopant coupled with the blue emission from the host by partial energy transfer.[22] In contrast to the devices based on **3**, in which the 4 wt % doping level achieved the best performance, the devices using **4** as dopant showed improved performance with increasing doping concentration (Fig. 11 and Table 3). The highest radiance (5238 Cd m^{-2} at 132 mA cm^{-2}, CIE coordinates $x = 0.41$, $y = 0.51$), maximum luminance efficiency (10.57 Cd A^{-1} at 1.38 mA cm^{-2}), and power efficiency (4.11 lm W^{-1} at 0.83 mA cm^{-2}) are attained by using emitter **4** at a 10 wt % doping level.

Comparing the EL spectra of **3** and **4**, the emissions contributing from excimers in **4** are significantly larger than those in **3** at high doping levels. The facile formation of excimers for complex **4** is presumably due to the stronger intermolecular interactions as revealed before in the crystal-structure section, which promotes the molecular aggregations.

Table 3. EL performance of devices doped with Ir^{III} and Pt^{II} complexes at different concentrations.

	$Ir(2\text{-PEC})_2(acac)$		$Ir(3\text{-PEC})_2(acac)$	
	3 wt %	7 wt %	3 wt %	7 wt %
L [cd·m^{-2}] [a]	1692	1232	3746	5319
L_{max} [cd·m^{-2}]	8926	4906	16632	25811
η_c [cd·A^{-1}] [a]	8.27	5.86	18.72	25.60
η_c [cd·A^{-1}] [b]	5.39	4.19	12.34	18.01
$\eta_{c,max}$ [cd·A^{-1}]	12.18	7.98	29.52	31.60
η_p [lm·W^{-1}] [a]	1.70	0.88	4.05	6.41
$\eta_{p,max}$ [lm·W^{-1}]	4.63	3.40	15.64	19.03
$\eta_{ext,max}$ [%]	7.35	4.81	8.25	11.02
V [a]	15.3	21.1	14.5	12.9
V_{ON} V	4.7	6.9	4.3	3.1
CIE (x,y)	0.63, 0.37	0.65, 0.35	0.29, 0.63	0.29, 0.63

	Pt(2-PEC)(acac)				Pt(3-PEC)(acac)			
	2 wt %	4 wt %	6 wt %	8 wt %	2 wt %	5 wt %	8 wt %	10 wt %
L [cd·m^{-2}] [a]	1415	3205	1352	1695	235	506	1154	1749
L_{max} [cd·m^{-2}]	3966	10265	3974	5928	922	1624	4953	5238
η_c [cd·A^{-1}] [a]	6.91	15.96	6.56	8.34	0.81	2.53	5.71	8.54
η_c [cd·A^{-1}] [b]	3.64	8.41	3.55	5.03	1.12	1.52	4.24	4.93
$\eta_{c,max}$ [cd·A^{-1}]	8.95	35.82	9.51	9.35	1.16	3.51	5.94	10.57
η_p [lm·W^{-1}] [a]	1.56	3.82	1.12	1.73	0.27	0.63	1.10	2.05
$\eta_{p,max}$ [lm·W^{-1}]	2.71	25.00	2.16	2.38	0.36	1.39	1.44	4.11
$\eta_{ext,max}$ [%]	2.65	13.10	3.62	3.80	0.51	1.24	1.99	–
V [a]	13.9	13.1	18.7	15.1	13.3	12.7	16.3	13.1
V_{ON} V	5.9	4.3	6.3	7.3	7.5	5.5	8.3	4.3
CIE (x,y)	0.42, 0.49	0.48, 0.48	0.53, 0.47	0.53, 0.46	0.17, 0.31	0.27, 0.50	0.45, 0.52	0.41, 0.51

[a] Recorded at 20 mA cm^{-2}. [b] Recorded at 100 mA cm^{-2}.

3. Conclusion

In conclusion, we have developed four novel carbazole-based heavy metal complexes in which the hole-transporting and electroluminescent functional groups are integrated into one molecule. The four complexes exhibit emission from blue–green to red light in both PL and EL. The remarkable color tuning is realized by linkage isomers in which iridium or platinum ligates with carbon at the 2- or 3-position of the carbazole unit. To our knowledge, this is the first report to utilize the electronic effect of carbon atoms at different positions of the carbazole unit to tune the energy gap and emission of metal complexes, which represents an alternative for color tuning of phosphorescent heavy metal complexes. Finally, we have demonstrated highly efficient OLEDs using these carbazole-based complexes as phosphorescent dyes. A green-light-emitting OLED device, with a maximum brightness of 25 811 Cd m^{-2}, a maximum luminance efficiency of 31.60 Cd A^{-1}, and power efficiency of 19.03 lm W^{-1} has been achieved by using iridium complex **2** as dopant. An orange-light-emitting OLED device, with a highest brightness of 10 265 Cd m^{-2}, a maximum luminance efficiency of 35.82 Cd A^{-1}, and a power efficiency of 25.00 lm W^{-1} has been fabricated by applying platinum complex **3** as the phosphorescent emitter. The outstanding device performance indicates the advantage of the ligand frame containing the carbazole unit, which may mainly contribute to an improved hole-transporting ability.

4. Experimental

4.1. General Information

2-bromo-*N*-ethylcarbazole and 3-bromo-*N*-ethylcarbazole were synthesized according to literature procedures [23]. 2-bromopyridine, *n*-butyllithium, anhydrous zinc chloride, and tetrakis(triphenylphosphine)palladium were purchased from Acros. Solvents were dried using standard procedures. ^{1}H NMR spectra were measured on a MECUYR-VX300 spectrometer in $CDCl_3$ using tetramethylsilane as an internal reference. Elemental analyses of carbon, hydrogen, and nitrogen were performed on a Carlorerba-1106 microanalyzer. Mass spectra were measured on a ZAB 3F-HF mass spectrophotometer. UV-vis absorption spectra were recorded on a Shimadzu 160A recording spectrophotometer. PL spectra were recorded on a Perkin-Elmer LS 55 luminescence spectrophotometer.

4.2. Electrochemistry

Cyclic voltammetry (CV) was carried out in nitrogen-purged anhydrous THF or dichloromethane at room temperature with a CHI voltammetric analyzer. Tetrabutylammonium hexafluorophosphate ($TBAPF_6$) (0.1 M) was used as the supporting electrolyte. The conventional three-electrode configuration consisted of a platinum working

ADVANCED FUNCTIONAL MATERIALS

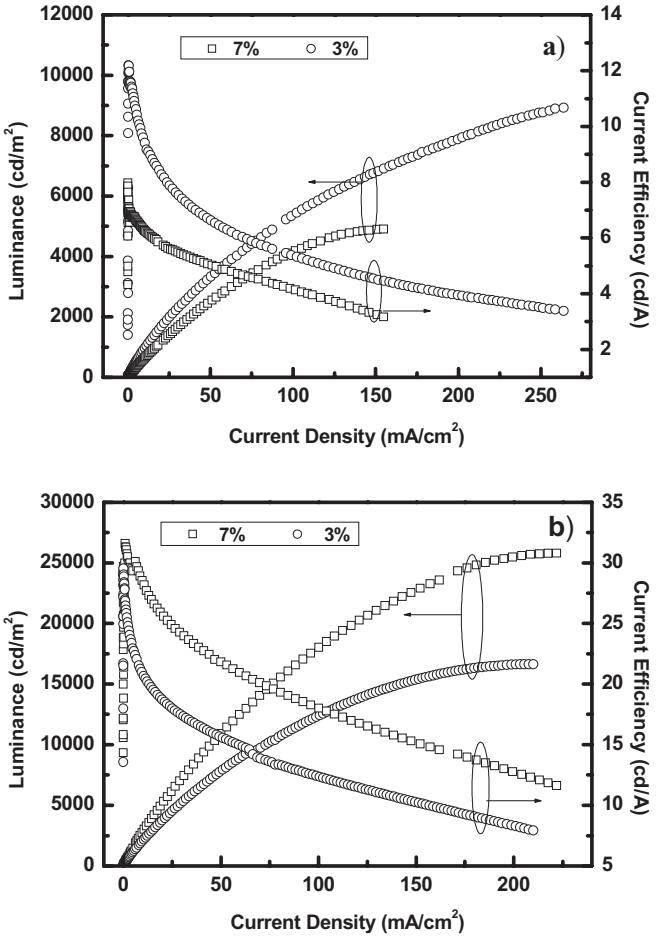

Figure 8. The luminance–current-density–luminance-efficiency (L–J–η_c) characteristics of an OLED device using a) **1** and b) **2** as dopant at different doping levels.

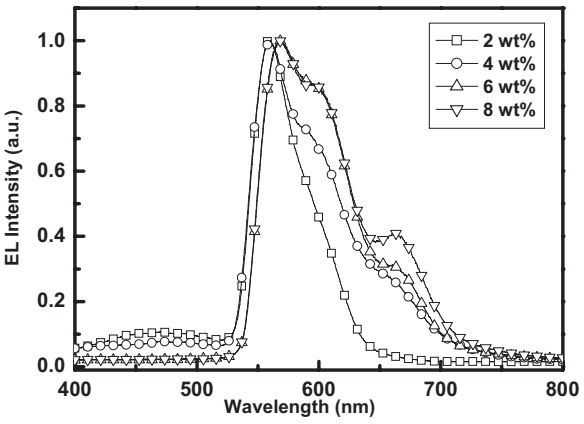

Figure 9. EL spectra of OLED devices using **3** as dopant at different doping concentrations.

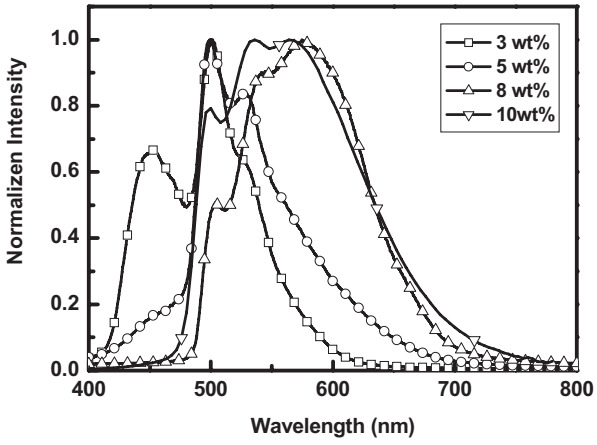

Figure 10. EL spectra of OLED devices using **4** as dopant at different doping concentrations.

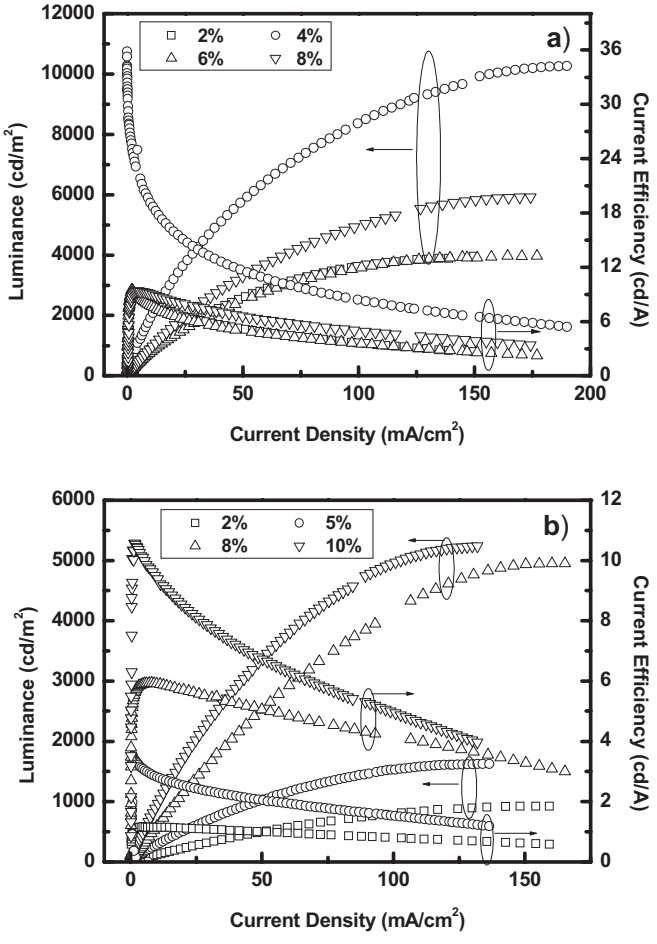

Figure 11. The luminance–current-density–luminance-efficiency (L–J–η_c) characteristics of OLED devices using a) **3** and b) **4** as dopant at different doping levels.

electrode, a platinum wire auxiliary electrode, and a Ag wire pseudo-reference electrode with the ferrocenium/ferrocene (Fc^+/Fc) couple as the internal standard. Cyclic voltammograms were obtained at a scan rate of 100 $mV\,s^{-1}$. Formal potentials are calculated as the average of cyclic voltammetric anodic and cathodic peaks.

4.3. Compounds

2-Pyridinyl-N-ethylcarbazole: *n*-BuLi (2.5 M in hexane, 4.0 mL, 9.4 mmol) was added dropwise to a solution of 2-bromopyridine (0.47 mL, 4.7 mmol) in 7.5 mL of anhydrous THF at –78 °C. After this mixture had been stirred at –78 °C for 45 min, a solution of anhydrous $ZnCl_2$ (1.28 g, 9.4 mmol) in 15 mL of THF was added slowly and stirred for 1.5 h at room temperature. Then a solution of 2-bromo-*N*-ethylcarbazole (1.27 g, 4.6 mmol) and $Pd(PPh_3)_4$ (55.3 mg, 0.05 mmol) in 15 mL of THF was added, and the mixture was refluxed under an argon atmosphere for 16 h. After cooling to room temperature, an aqueous solution of NH_4Cl (2.2 g, 41 mmol) was added. Then the mixture was stirred for 15 min and extracted several times with CH_2Cl_2 and dried over Na_2SO_4. The pure product was obtained after column chromatography on silica gel using chloroform and petroleum ether (1:10) as the eluent. Yield: 80 %. IR (cm^{-1}): 2917(s), 2845(s), 1589(m), 1449(s), 1327(m), 1344(m). ^1H NMR($CDCl_3$, 300 MHz) *d* [ppm]: 8.75 (d, $J = 4.5$ Hz, 1H), 8.19–8.12 (m, 3H), 7.88 (d, $J = 8.4$ Hz, 1H), 7.82–7.77 (m, 2H), 7.53–7.42 (m, 2H), 7.27–7.23 (m, 2H), 4.47 (q, $J = 7.2$ Hz, 2H), 1.48 (t, $J = 7.2$ Hz, 3H).

3-Pyridinyl-N-ethylcarbazole: This compound was synthesized according to the above method except for using 3-bromo-*N*-ethylcarbazole as opposed to 2-bromo-*N*-ethylcarbazole. Yield: 66 %. IR (cm^{-1}): 2926(s), 2854(s), 1716(m), 1587(s), 1466(s), 1438(s), 1350(m), 1327(m), 1255(m). ^1H NMR ($CDCl_3$, 300 MHz) *d*[ppm]: 8.79–8.72 (m, 1H), 8.21–8.14 (m, 2H), 7.79 (d, $J = 8.1$ Hz, 1H), 7.80 (t, $J = 6.9$ Hz, 1H), 7.51–7.42 (m, 3H), 7.29–7.21 (m, 3H), 4.41 (q, $J = 7.2$ Hz, 2H), 1.47 (t, $J = 7.2$ Hz, 3H).

*Complexes **1** and **2***: A mixture of ligand 2-PEC or 3-PEC (0.39 g, 1.42 mmol), $IrCl_3{\cdot}3H_2O$ (0.21 g, 0.59 mmol), 2-ethoxyethanol (12 mL) and distilled water (4 mL) was stirred under argon at 120 °C for 24 h. After cooling, the resulting precipitate was collected by filtration and washed with water, ethanol, and hexane successively. The dried chloro-bridged dimer (0.12 g, 0.08 mmol) was suspended in 2-ethoxyethanol (8 mL) and treated with acetylacetone (0.24 mmol) and anhydrous Na_2CO_3 (86 mg, 0.8 mmol). The mixture was stirred under argon at 100 °C for 16 h. After cooling to room temperature, the resulting precipitate was filtered off and washed with water, ethanol, and hexane. The crude product was purified by flash chromatography on silica gel using CH_2Cl_2 as the eluent to afford the desired Ir^{III} complex.

*Ir(2-PEC)$_2$(acac) (**1**)*: Yield: 58 %. ^1H NMR ($CDCl_3$, 300 MHz) *d*[ppm]: 8.66 (d, $J = 5.4$ Hz, 2H), 8.07 (d, $J = 8.1$ Hz, 2H), 7.83 (t, $J = 8.1$ Hz, 2H), 7.63 (m, 4H), 7.26–7.13 (m, 6H), 6.94 (t, $J = 8.1$ Hz, 2H), 6.86 (m, 4H), 5.26 (s, 1H), 3.90 (q, $J = 6.3$ Hz, 4H), 1.81 (s, 6H), 1.35 (t, $J = 6.3$ Hz, 6H). Anal. calcd. for $C_{43}H_{37}IrN_4O_2$: C 61.93, H 4.47, N 6.72. Found: C 61.47, H 4.32, N 6.55. MS (FAB): *m*/*z*: 834 (M^+).

*Ir(3-PEC)$_2$(acac) (**2**)*: Yield: 53 %. ^1H NMR ($CDCl_3$, 300 MHz) *d*[ppm]: 8.59 (d, $J = 5.1$ Hz, 2H), 8.29 (s, 2H), 8.04 (d, $J = 7.5$ Hz, 2H), 7.93 (d, $J = 7.5$ Hz, 2H), 7.90 (t, $J = 7.2$ Hz, 2H), 7.24 (t, $J = 7.5$ Hz, 2H), 7.13 (m, 4H), 7.06 (t, $J = 7.2$ Hz, 2H), 6.16 (s, 2H), 5.26 (s, 1H), 3.90 (q, $J = 6.9$ Hz, 4H), 1.82 (s, 6H), 1.34 (t, $J = 6.9$ Hz, 6H). Anal. calcd. for $C_{43}H_{37}IrN_4O_2$:C 61.93, H 4.47, N 6.72. Found: C 61.55, H 4.21, N 6.70. MS (FAB): *m*/*z*: 834 (M^+).

*Complexes **3** and **4***: The two platinum complexes were prepared according to the similar method as before except for using K_2PtCl_4 (0.24 g 0.59 mmol) to replace $IrCl_3{\cdot}nH_2O$.

*Pt(2-PEC)(acac) (**3**)*: Yield: 68 %. ^1H NMR ($CDCl_3$, 300 MHz) *d*[ppm]: 9.03 (d, $J = 5.1$ Hz, 1H), 8.22 (s, 1H), 8.05 (d, $J = 8.4$ Hz, 1H), 7.79 (m, 2H), 7.51 (s, 1H), 7.44 (t, $J = 7.2$ Hz, 1H), 7.34 (d, $J = 7.8$ Hz, 1H),7.18 (t, $J = 6.3$ Hz, 1H), 7.09 (m, 1H), 5.50 (s, 1H), 4.37 (q, 2H), 2.10 (s, 3H), 2.01 (s, 3H), 1.45 (t, $J = 6.3$ Hz, 3H). Anal. calcd. for $C_{24}H_{22}N_2O_2Pt$: C 50.97, H 3.92, N 4.95. Found: C 50.53, H 3.66, N 4.99. MS (FAB): *m*/*z*: 565 (M^+).

*Pt(3-PEC)(acac) (**4**)*: Yield: 70 %. ^1H NMR ($CDCl_3$, 300 MHz) *d*[ppm]: 8.94 (d, $J = 5.1$ Hz, 1H), 8.19 (s, H), 8.05 (d, $J = 6.6$ Hz, 1H), 7.75 (m, 2H), 7.55 (s, 1H), 7.42 (t, $J = 7.2$ Hz, 1H), 7.36 (d, $J = 8.1$ Hz, 1H), 7.20 (t, $J = 7.2$ Hz, 1H), 7.02 (m, 1H), 5.50 (s, 1H), 4.88 (q, 2H), 2.07 (s, 3H), 2.02 (s, 3H), 1.48 (t, $J = 7.2$ Hz, 3H). Anal. calcd. for $C_{24}H_{22}N_2O_2Pt$: C 50.97, H 3.92, N 4.95. Found: C 50.75, H 3.65, N 5.11. MS (FAB): *m*/*z*: 565 (M^+).

4.4. X-ray Structural Analysis

Single-crystal X-ray diffraction data were obtained on a Bruker AXS Smart CCD diffractometer using a graphite monochromated Mo Kα ($\lambda = 0.71073$ Å) radiation. The data were collected using the $\omega/2\theta$ scan mode and corrected for Lorentz and polarization effects, during data reduction using Shelxtl 97 software the absorption effect was corrected for as well.

Crystallographic data for the structural analyses have been deposited with the Cambridge Crystallographic Data Center (CCDC). CCDC reference numbers for **1**, **3**, and **4** are 615474, 615476, and 615475, respectively. Copies of this information can be obtained free of charge from The Director, CCDC, 12 Union Road, Cambridge, CB2 1EZ, UK (Fax: +441223336033; E-mail: deposit@ccdc.cam.ac.uk, or www: http://www.ccdc.cam.ac.uk).

4.5. Density Functional Theory Calculations

The ground-state geometries of the complexes were fully optimized without symmetry constraints using the B3LYP density-functional theory and the "double-ξ" quality basis sets for the ligand (6-31g) and the Ir(LANL2DZ) or the Pt(LANL2DZ) sets for the metal complexes [24]. Then, time-dependent DFT (TDDFT) calculations using B3LYP density functional theory and "double-ξ" quality basis sets for the ligand (6-31g) and Ir(LANL2DZ) or the Pt(LANL2DZ) were performed [25]. All these were carried out with the Gaussian 03 package [26].

4.6. OLED Fabrication and Measurements

The organic layers and metal cathode were fabricated by high-vacuum thermal evaporation onto a pre-cleaned indium tin oxide (ITO) glass substrate. In a vacuum chamber with a pressure of $< 10^{-4}$ Pa, the following components were sequentially deposited onto the substrate to construct the device: 40 nm of 4,4′-bis[*N*-(1-naphthyl)-*N*-phenylamino]biphenyl (NPB) as the hole-transporting layer, 30 nm of the complex doped 4,4′-biscarbazolybiphenyl (CBP) as the emitting layer, 20 nm of 2,9-dimethyl-4,7-diphenyl-1,10-phenanthroline (BCP) as a hole- and exciton-blocking layer, 30 nm of AlQ_3 as the electron-transporting layer, and a cathode composed of 1 nm of lithium fluoride and 100 nm of aluminum. The current–voltage-brightness (*I*–*V*–*B*) characteristics of EL devices were measured at ambient condition with a Keithey 2400 Source meter and a Keithey 2000 Source multimeter equipped with a calibrated silicon photodiode. The EL spectra were measured by a JY SPEX CCD3000 spectrometer.

Received: July 24, 2006
Revised: September 18, 2006
Published online: January 24, 2007

[1] a) C. W. Tang, S. A. VanSlyke, *Appl. Phys. Lett.* **1987**, *51*, 913. b) J. H. Burroughes, D. D. C. Bradley, A. R. Brown, R. N. Marks, K. Mackay, R. H. Friend, P. L. Burns, A. B. Holmes, *Nature* **1990**, *347*, 539.

[2] a) M. A. Baldo, S. Lamansky, P. E. Burrows, M. E. Thompson, S. R. Forrest, *Appl. Phys. Lett*. **1999**, *75*, 4. b) C. Adachi, M. A. Baldo, S. R. Forrest, M. E. Thompson, *Appl. Phys. Lett*. **2000**, *77*, 904. c) M. Ikai, S. Tokito, Y. Sakamoto, T. Suzuki, Y. Taga, *Appl. Phys. Lett*. **2001**, *79*, 156. d) S. Lamansky, P. Djurovich, D. Murphy, F. Abdel-Razzaq,

H. E. Lee, C. Adachi, P. E. Buttows, S. R. Forrest, M. E. Thompson, *J. Am. Chem. Soc.* **2001**, *123*, 4304. e) M. K. Nazeeruddin, R. Humphry-Baker, D. Berner, S. Rivier, L. Zuppiroli, M. Graetzel, *J. Am. Chem. Soc.* **2003**, *125*, 8790. f) J. Kim, I. S. Shin, H. Kim, J. K. Lee, *J. Am. Chem. Soc.* **2005**, *127*, 1614.

[3] a) M. A. Baldo, D. F. O'Brien, Y. You, A. Shoustikov, S. Sibley, M. E. Thompson, S. R. Forrest, *Nature* **1998**, *395*, 151. b) R. C. Kwong, S. Sibley, T. Dubovoy, M. Baldo, S. R. Forrest, M. E. Thompson, *Chem. Mater.* **1999**, *11*, 3709. c) W. Lu, B. X. Mi, M. C. W. Chan, Z. Hui, N. Zhu, S. T. Lee, C. M. Che, *Chem. Commun*. **2002**, 206. d) J. Brooks, Y. Babayan, S. Lamansky, P. I. Djurovich, M. E. Thompson, *Inorg. Chem*. **2002**, *41*, 3055.

[4] a) X. Jiang, A. K.-Y. Jen, B. Carlson, L. R. Dalton, *Appl. Phys. Lett.* **2002**, *80*, 713. b) B. Carlson, G. D. Phelan, W. Kaminsky, L. Dalton, X. Jiang, M. S. Liu, A. K.-Y. Jen, *J. Am. Chem. Soc.* **2002**, *124*, 14 162. c) J. H. Kim, M. S. Liu, A. K.-Y. Jen, B. Carlson, L. R. Dalton, C.-F. Shu, R. Dodda, *Appl. Phys. Lett.* **2003**, *83*, 776. d) Y.-M. Cheng, Y.-S. Yeh, M.-L. Ho, P.-T. Chou, *Inorg. Chem*. **2005**, *44*, 4594.

[5] a) S. Bernhard, J. A. Barron, P. L. Houston, H. D. Abruna, J. L. Ruglovksy, X. Gao, G. G. Malliaras, *J. Am. Chem. Soc.* **2002**, *124*, 13 624. b) M. Buda, G. Kalyuzhny, A. J. Bard, *J. Am. Chem. Soc.* **2002**, *124*, 6090.

[6] a) X. Gong, P. K. Ng, W. K. Chan, *Adv. Mater.* **1998**, *10*, 1337. b) W. K. Chan, P. K. Ng, X. Gong, S. Hou, *Appl. Phys. Lett.* **1999**, *75*, 3920. c) K. Wang, L. Huang, L. Gao, L. Jin, C. Huang, *Inorg. Chem*. **2002**, *41*, 3353.

[7] a) Y. Cao, I. D. Parker, A. J. Heeger, *Nature* **1999**, *397*, 414. b) M. Wohlgenannt, K. Tandon, S. Mazumdar, S. Ramasesha, Z. V. Vardeny, *Nature* **2001**, *409*, 494.

[8] R. A. Campos, I. P. Kovalev, Y. Guo, N. Wakili, T. Skotheim, *J. Appl. Phys.* **1996**, *80*, 7144.

[9] a) M. R. Robinson, M. B. O'Regan, G. C. Bazan, *Chem. Commun*. **2000**, 1645. b) H. Xin, F. Li, M. Shi, Z. Bian, C. Huang, *J. Am. Chem. Soc.* **2003**, *125*, 7166. c) F. Liang, Q. Zhou, Y. Cheng, L. Wang, D. Ma, X. Jing, F. Wang, *Chem. Mater.* **2003**, *15*, 1935.

[10] a) W.-Y. Wong, Z. He, S.-K. So, K.-L. Tong, Z. Lin, *Organometallics* **2005**, *24*, 4079. b) W.-Y. Wong, G.-J. Zhou, X.-M. Yu, H.-S. Kwok, B.-Z. Tang, *Adv. Funct. Mater*. **2006**, *16*, 838. c) L. Chen, C. Yang, J. Qin, J. Gao, H. You, D. Ma, *J. Organomet. Chem*. **2006**, *391*, 3519. d) Z. Liu, M. Guan, Z. Bian, D. Nie, Z. Gong, Z. Li, C. Huang, *Adv. Funct. Mater*. **2006**, *16*, 1441. e) L. Chen, H. You, C. Yang, X. Zhang, J. Qin, D. Ma, *J. Mater. Chem.* **2006**, *16*, 3332.

[11] a) Y. J. Su, H. L. Huang, C. L. Li, C. H. Chien, Y. T. Tao, P. T. Chou, S. Datta, R. S. Liu, *Adv. Mater.* **2003**, *15*, 884. b) C. H. Yang, C. C. Tai, I. W. Sun, *J. Mater. Chem.* **2004**, *14*, 947. c) I. R. Laskar, T. M. Chen, *Chem. Mater.* **2004**, *16*, 111. d) W. S. Huang, J. T. Lin, C. H. Chien, Y. T. Tao, S. S. Sun, Y. S. Wen, *Chem. Mater.* **2004**, *16*, 2480. e) V. V. Grushin, N. Herron, D. D. LeCloux, W. J. Marshall, V. A. Petrov, Y. Wang, *Chem. Commun.* **2001**, 1494. f) P. Coppo, E. A. Plummer, L. de Cola, *Chem. Commun*. **2004**, 1774.

[12] Q. D. Liu, R. Y. Wang, S. N. Wang, *Dalton Trans.* **2004**, 2073.

[13] S. Lamansky, P. I. Djurovich, F. Abdel-Razzaq, S. Garon, D. L. Murphy, M. E. Thompson, *J. Appl. Phys.* **2002**, *92*, 1570.

[14] J. F. Ambrose, L. L. Carpenter, R. F. Nelson, *J. Electrochem. Soc.* **1975**, *122*, 876.

[15] K. Brunner, A. V. Dijken, H. Borner, J. J. Bastiaansen, N. M. Kiggen, B. M. Langeveld, *J. Am. Chem. Soc.* **2004**, *126*, 6035.

[16] a) A. Chen, J. Liao, Y. Liang, M. O. Ahmed, H. Tseng, S. Chen, *J. Am. Chem. Soc.* **2003**, *125*, 636. b) J.-F. Morin, N. Drolet, Y. Tao, M. Leclerc, *Chem. Mater*. **2004**, *16*, 4619. c) M. Sonntag, P. Strohriegl, *Chem. Mater*. **2004**, *16*, 4736. d) J.-F. Morin, M. Leclerc, *Macromolecules* **2002**, *35*, 8413.

[17] M. Nonoyama, *Bull. Chem. Soc. Jpn*. **1974**, *47*, 767.

[18] A. S. Ionkin, W. J. Marshall, Y. Wang, *Organometallics* **2005**, *24*, 619.

[19] J. Li, P. I. Djurovich, B. D. Alleyne, M. Yousufuddin, N. N. Ho, J. C. Thomas, J. C. Peters, R. Bau, M. E. Thompson, *Inorg. Chem*. **2005**, *44*, 1713.

[20] H.-C. Li, P.-T. Chou, Y.-H. Hu, Y.-M. Cheng, R.-S. Liu, *Organometallics* **2005**, *24*, 1329.

[21] S. Lamansky, P. Djurovich, D. Murphy, F. Abdel-Razzaq, R. Kwong, I. Tsyba, M. Bortz, B. Mui, R. Bau, M. E. Thompson, *Inorg. Chem*. **2001**, *40*, 1704.

[22] a) C.-M. Che, S.-C. Chan, H.-F. Xiang, M. C. W. Chan, Y. Liu, Y. Wang, *Chem. Commun.* **2004**, 1484. b) W. Lu, B.-X. Mi, M. C. W. Chan, Z. Hui, C.-M. Che, N. Zhu, S.-T. Lee, *J. Am. Chem. Soc.* **2004**, *126*, 4958.

[23] A. Lützen, M. Hapke, *Eur. J. Org. Chem.* **2002**, 2292.

[24] a) C. Lee, W. Yang, R. G. Parr, *Phys. Rev. B* **1988**, *37*, 785. b) A. D. Becke, *J. Chem. Phys.* **1993**, *98*, 5648.

[25] a) C. Jamorski, M. E. Casida, D. R. Salahub, *J. Chem. Phys.* **1996**, *104*, 5134. b) M. Petersilka, U. J. Grossmann, E. K. U. Gross, *Phys. Rev. Lett*. **1996**, *76*, 1212. c) R. Bauernschmitt, R. Ahlrichs, F. H. Hennrich, M. M. Kappes, *J. Am. Chem. Soc.* **1998**, *120*, 5052. d) M. E. Casida, *J. Chem. Phys.* **1998**, *108*, 4439. e) R. E. Stratmann, G. E. Scuseria, M. J. Frisch, *J. Chem. Phys.* **1998**, *109*, 8218.

[26] M. J. Frisch, G. W. Trucks, H. B. Schlegel, G. E. Scuseria, M. A. Robb, J. R. Cheeseman, J. A. Montgomery, Jr., T. Vreven, K. N. Kudin, J. C. Burant, J. M. Millam, S. S. Iyengar, J. Tomasi, V. Barone, B. Mennucci, M. Cossi, G. Scalmani, N. Rega, G. A. Petersson, H. Nakatsuji, M. Hada, M. Ehara, K. Toyota, R. Fukuda, J. Hasegawa, M. Ishida, T. Nakajima, Y. Honda, O. Kitao, H. Nakai, M. Klene, X. Li, J. E. Knox, H. P. Hratchian, J. B. Cross, V. Bakken, C. Adamo, J. Jaramillo, R. Gomperts, R. E. Stratmann, O. Yazyev, A. J. Austin, R. Cammi, C. Pomelli, J. W. Ochterski, P. Y. Ayala, K. Morokuma, G. A. Voth, P. Salvador, J. J. Dannenberg, V. G. Zakrzewski, S. Dapprich, A. D. Daniels, M. C. Strain, O. Farkas, D. K. Malick, A. D. Rabuck, K. Raghavachari, J. B. Foresman, J. V. Ortiz, Q. Cui, A. G. Baboul, S. Clifford, J. Cioslowski, B. B. Stefanov, G. Liu, A. Liashenko, P. Piskorz, I. Komaromi, R. L. Martin, D. J. Fox, T. Keith, M. A. Al-Laham, C. Y. Peng, A. Nanayakkara, M. Challacombe, P. M. W. Gill, B. Johnson, W. Chen, M. W. Wong, C. Gonzalez, J. A. Pople, *Gaussian 03, Revision C.02*, Gaussian, Inc., Wallingford, CT, **2004**.